Capillarity

Vol. 18, No. 1, p. 14-26, 2026

Original article

Molecular insights into interfacial behavior of crude oil-brine-quartz systems under brine dilution

Zhilin Cheng[1]*, Minrong Xiao[1], Shaokai Tong[2], Shuang Zhang[3], Yuxin Miao[1], Meng Xiao[1]

[1]*School of Petroleum Engineering, Xi'an Shiyou University, Xi'an 710065, P. R. China*

[2]*Changqing Downhole Technology Company, CNPC Chuanqing Drilling Engineering Company, Xi'an 710021, P. R. China*

[3]*Research Institute of Exploration & Development, PetroChina Liaohe Oilfield Company, Panjin 124010, P. R. China*

Keywords:
Quartz
wettability
brine dilution
molecular dynamics

Cited as:
Cheng, Z., Xiao, M., Tong, S., Zhang, S., Miao, Y., Xiao, M. Molecular insights into interfacial behavior of crude oil-brine-quartz systems under brine dilution. Capillarity, 2026, 18(1): 14-26.
https://doi.org/10.46690/capi.2026.01.02

Abstract:
The influence of brine dilution on interfacial behavior in sandstone reservoirs remains inadequately understood. In this study, molecular dynamics simulations were conducted to elucidate the effects of brine dilution on the wetting behavior of three crude oil systems containing O-, N- and S-bearing heteroatoms. Quartz was adopted as a model sandstone mineral, and the investigation centered on contact angles, fluid density distributions, radial distribution functions, interaction energies, and hydrogen-bonding interactions. The results showed that decreasing brine salinity enhanced quartz hydrophilicity. Contact angles decreased with dilution in O- and N-bearing oils, while the S-bearing system exhibited a non-monotonic trend; however, the overall changes were minor. A water film consistently formed between oil droplets and quartz, thickening with decreasing salinity, which lowered oil-quartz interaction and crude oil density near the surface. Alkanes tended to deplete near the interface, while aromatics preferentially accumulated in this region, although a portion of the aromatics could still migrate into the bulk phase. The relationship between near-wall non-hydrocarbon density and contact angle varied by oil type – positive for O- and S-containing oils, negative for N-containing oils. Brine dilution also strengthened water-quartz interactions through increased hydrogen bonding, further reducing oil adhesion. Despite these effects, the contact angles in all systems exhibited minimal changes upon brine dilution and remained within the strongly water-wet state. Thus, in reservoirs with inherent water-wet conditions, brine dilution alone is unlikely to significantly enhance oil recovery.

1. Introduction

Given the abundant reserves and widespread distribution of sandstone reservoirs, their efficient exploitation is critical for maintaining global oil and gas supply (Cai et al., 2021; Liu, 2023). Typically, after the primary and secondary recovery stages, nearly two-thirds of the original oil remains trapped within the reservoir. Tertiary recovery processes, such as chemical flooding, rely on the injection of targeted reagents to mobilize this residual oil (Dordzie and Dejam, 2021; Javadi and Fatemi, 2022; Oguntade et al., 2024; Wang and Chang, 2024). Among the various enhanced oil recovery techniques, low-salinity waterflooding (LSW) has emerged as a cost-effective, environmentally benign and operationally simple strategy that significantly enhances oil production in sandstone reservoirs (Almeida da Costa et al., 2020). Its high efficacy is largely attributed to its ability to alter reservoir

Yandy Scientific Press

*Corresponding author.
E-mail address: zcheng21@xsyu.edu.cn (Z. Cheng); rongrong20220120@163.com (M. Xiao); sktong1987@126.com (S. Tong); lh_zhangshuang@petrochina.com.cn (S. Zhang); myxxsyu@163.com (Y. Miao); abc772432442@hotmail.com (M. Xiao).

Received November 16, 2025; revised December 12, 2025; accepted January 1, 2026; available online January 3, 2026.

wettability toward a more water-wet state (Ghasemi and Shafiei, 2022; Arain et al., 2024).

With ongoing research, the mechanism by which LSW technology alters the wettability of sandstone reservoirs has become an emerging subject. Currently, researchers primarily explore the underlying mechanisms through macroscopic experimental methods centered on contact angle measurements (Bhutto et al., 2022; Alomair et al., 2023; Gómez-Delgado et al., 2023), and microscopic techniques such as molecular dynamics (MD) simulations (Koleini et al., 2019; Seyyedattar et al., 2019; Shi et al., 2023; Cai et al., 2024). However, this experimental method falls short of providing microscale insights into the interfacial behaviors of complex fluid-solid systems (Pan et al., 2024; Fang et al., 2025). In contrast, the MD method provides real-time tracking of atomic trajectories, enabling the visual representation of multi-component dynamic behaviors. Accordingly, it has been widely used to investigate the influence of brine salinity, ionic composition, mineral type, and thermobaric conditions on wettability (Cui et al., 2022; Liu et al., 2023; Chen et al., 2024; Singh et al., 2024; Tian et al., 2024). On the other hand, quartz – as the primary mineral type in sandstone – is the most frequently used mineral in most MD studies. For example, Fang et al. (2020) employed n-dodecane as a model oil and demonstrated that LSW enhances oil desorption by thickening the interfacial water film, with changes in the chemical potential of water molecules driving wettability alteration. However, their study was limited to a single crude oil model. Sun et al. (2021) further explored the effects of ion type using a composite crude oil model containing stearic acid, demonstrating that calcium-rich brines promote the adsorption of polar acidic molecules onto quartz surfaces via cation bridging. Conversely, sodium-rich brines enhance the water-wetness of the quartz substrate by displacing calcium ions, thereby reducing oil affinity. Furthermore, Chen and Singer (2019) employed molecular dynamics simulations to investigate how changes in the salinity of sodium chloride brine affect its hydrophilicity. The results indicated that variations in brine salinity alter the electric double layer structure on quartz surfaces, thereby influencing surface properties. However, the simplistic brine model they used fails to adequately account for critical factors such as the coexistence of multiple ions and complex compositions found in reservoir environments, a limitation that restricts the generalizability of the research conclusions. Recognizing the complexity of reservoir environments, Wang and Chang (2024) investigated the combined effects of temperature, pressure and pore size on the wettability of octane on calcite. Their analysis of intercomponent adsorption energies revealed that temperature and mineralogy are dominant factors, whereas pressure exerts a relatively minor influence. Despite the substantial progress, most MD-based studies employ overly simplified crude oil models (Ghasemi et al., 2022), often neglecting the multicomponent nature of real oil systems. Furthermore, prior research has largely focused on single or binary salt systems, limiting the mechanistic understanding of induced change in wetting behaviors under realistic conditions (Ghasemi et al., 2022).

To address the above gaps, the present study developed a representative sandstone reservoir model incorporating quartz substrates and three multicomponent crude oil models. Nonane and toluene were used to represent alkanes and aromatics, while mercaptan, pyridine and acetic acid served as non-hydrocarbon functional groups. To capture the full image of salinity effects, realistic formation water and its serial dilutions at various concentrations were included. Through MD simulations, the interfacial behavior and wettability mechanisms were systematically investigated across crude oil-brine-quartz systems. The paper is structured as follows: Section 2 details the simulation methodology, Section 3 presents and interprets the results based on density distributions, radial distribution functions, interaction energies, and hydrogen bonding analysis, and Section 4 summarizes the key conclusions.

2. Simulation methodology

2.1 Model construction

Quartz, as the dominant mineral constituent in sandstone reservoirs, is widely employed as a model substrate for investigating surface wettability via molecular simulation (Deng et al., 2023; Kobayashi and Firoozabadi, 2024; Cheng et al., 2025; Khovental et al., 2025). To more accurately replicate reservoir conditions and capture interfacial interactions at the mineral-fluid interface, a hydroxylated α-quartz slab was constructed by expanding a unit cell to dimensions of approximately 3.3 nm $\times$ 17.1 nm $\times$ 1.6 nm along the x, y and z directions, respectively.

To develop a realistic representation of light crude oil, nonane and toluene were selected as representative alkane and aromatic components, respectively, while mercaptan (S-containing), pyridine (N-containing) and acetic acid (O-containing) were incorporated as key non-hydrocarbon constituents (Kunieda et al., 2010; Tang et al., 2018; Aljamali and Salih, 2021). Three distinct polar crude oil models were formulated at a 40:10:3 molar ratio, derived from mass fraction analysis of typical crude oil compositions. To minimize the influence of line tension, the crude oil droplet was modeled as a cylindrical structure oriented along the x-axis and positioned near the quartz surface (Liu et al., 2024). Brine was placed surrounding the oil phase, with formation water salinity set at 58,746 mg/L, comprising primarily Na^+, Ca^{2+} and Cl^- ions (Cheng et al., 2024).

For systematic analysis, S-containing crude oil systems under original, 5-fold and 20-fold dilution conditions were labeled as S, S5 and S20, respectively. The same naming convention was applied to the remaining systems. The specific molecular compositions of the oil phases and the corresponding ion concentrations in each brine condition are summarized in Table 1, where X represents the crude oil system containing S, N, and O.

A total of nine systems were constructed for this study. As an illustrative example, the configuration of the O-containing crude oil-formation water-quartz system is presented in Fig. 1. To enable the application of reflective wall boundary conditions, a 2.6 nm vacuum layer was introduced above the fluid domain.

Table 1. Molecular and ionic composition of crude oil and brines.

System	Number of molecules or ions									
	Alkane	Aromatic	Non-hydrocarbon	H_2O	Na^+	Mg^{2+}	Ca^{2+}	Cl^-	SO_4^{2-}	HCO_3^-
X				15871	230	5	40	310	2	6
X5	200	50	15	15871	46	1	8	62	0	2
X20				15871	12	0	2	16	0	0

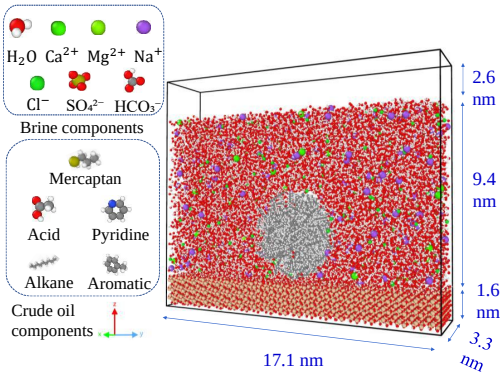

Fig. 1. Schematic illustration of the brine ionic composition, crude oil components, and quartz-(O-containing crude oil)-formation water system.

2.2 Simulation settings

All MD simulations were performed using the LAMMPS software package (Plimpton, 1995). The quartz substrate was modeled using the Interface force field developed by Heinz et al. (2013), which has been extensively validated for gas/liquid-solid interfacial behavior. Water molecules were described using the SPC/Fw model (Khalkhali et al., 2017; Tian and Wang, 2017; Zhan et al., 2020), while the OPLS-AA force field (Dastjerdi et al., 2024; Mohammed et al., 2025; Wang et al., 2025) was employed for both the oil molecules and the dissolved ions. These force fields have been widely adopted in previous investigations of interfacial wettability and fluid-solid interactions (Tian et al., 2019). The non-bonded interaction parameters for all species, including crude oil components, ions and quartz atoms, are summarized in Table 2.

The total non-covalent interactions between particles comprise short-range van der Waals forces and long-range electrostatic interactions. The short-range forces are represented by the 12-6 Lennard-Jones (LJ) potential (Lyu et al., 2024), while the electrostatic contributions are modeled using Coulomb interactions, as described in Eq. (1). Both interactions employ a cutoff radius of 1.2 nm. The LJ potential includes standard tail corrections, and long-range electrostatics are computed using the particle-particle particle-mesh method with a precision of 0.0001:

$$E_{ij} = 4\varepsilon_{ij}\left[\left(\frac{\sigma_{ij}}{r_{ij}}\right)^{12} - \left(\frac{\sigma_{ij}}{r_{ij}}\right)^{6}\right] + \frac{q_i q_j}{4\pi\varepsilon_0 r_{ij}} \quad (1)$$

$$\varepsilon_{ij} = \sqrt{\varepsilon_i \varepsilon_j}, \quad \sigma_{ij} = \sqrt{\sigma_i \sigma_j} \quad (2)$$

where E_{ij}, ε_{ij}, σ_{ij}, r_{ij}, ε_0, q_i, and q_j represent the total non-covalent interactions, the Lennard-Jones well depth, distance parameter, interparticle distance, vacuum permittivity, and the partial charges of particles i and j, respectively. The non-bonded interactions between dissimilar particles were evaluated using the geometric mixing rule, as given in Eq. (2). ε_i and ε_j represent the energy values of particles i and j, respectively, while σ_i, σ_j denote the distances between particles i and j in Eq. (2).

Periodic boundary conditions were applied along the x and y directions of the simulation box, while fixed boundaries with reflective walls were imposed along the z axis to prevent molecular escape. In addition, a 2.6 nm vacuum layer was introduced above the system to construct an open system exposed to vacuum, a commonly adopted approach in interfacial molecular simulations (Tian and Wang, 2017; Tian et al., 2019; Arboleda-Lamus et al., 2024). To constrain the quartz substrate, silicon and oxygen atoms were fixed in place, allowing only the surface hydroxyl hydrogen atoms to move freely (Tian and Wang, 2017; Fang et al., 2020). Prior to production runs, energy minimization was performed to eliminate unfavorable atomic contacts. The system was then equilibrated in the canonical ensemble at a reservoir temperature of 323.15 K, regulated by a Nosé-Hoover thermostat. MD simulations were conducted with a 1 fs time step over a total duration of 40 ns. The first 35 ns were used for equilibration, and the final 5 ns were allocated for data collection. System configurations were sampled every 1 ns to analyze molecular density profiles, radial distribution functions, intermolecular interaction energies, and related properties. Atomic trajectories were post-processed and visualized using the OVITO software (Stukowski, 2009).

Furthermore, to validate the reliability of our molecular simulations, they were performed for the water-decane interfacial tension as well as the contact angles of water-air-quartz and water-decane-quartz systems. These simulation results were compared with experimental data, confirming the accuracy of our force-field parameters and simulation setup. Detailed information can be found in the Supporting Materials.

2.3 Data post-processing

This section outlines the quantitative methods used to evaluate contact angles and hydrogen bonding. Based on the obtained atomic trajectories, two-dimensional density distribution maps of the oil phase were constructed, as illustrated in Fig. 2.

Table 2. Non-bonding interaction parameters for the crude oil-brine-quartz system.

Type	Atoms	ε (kcal/mol)	σ (Å)	q (e)
Na^+	Na	0.0005	4.0700	+1.0000
Cl^-	Cl	0.7100	4.0200	-1.0000
Ca^{2+}	Ca	0.4497	2.4120	+2.0000
Mg^{2+}	Mg	0.8750	1.6445	+2.0000
SO_4^{2-}	S	0.2000	3.5500	+2.0000
	O	0.1553	3.2500	-1.0750
HCO_3^-	O1	0.1553	3.2500	-1.0750
	C	0.0700	3.5500	+0.4970
	O2	0.1700	3.1200	-0.5708
	H	0.0000	0.0000	+0.3723
H_2O	Hw	0.0000	0.0000	+0.4100
	Ow	0.1554	3.1655	-0.8200
C_9H_{20}	C	0.0696	3.5	-0.1790
	H	0.03	2.5	+0.0891
C_7H_8	C1	0.0660	3.5000	-0.2390
	C2	0.0660	3.5000	-0.1794
	H1	0.0300	2.5000	+0.0883
	H2	0.0300	2.5000	+0.1210
C_3H_8S	C	0.0660	3.5000	-0.1838
	S	0.4250	3.6000	-0.2675
	H1	0.0300	2.5000	+0.1259
	H2	0.0000	0.0000	+0.1449
C_5H_5N	C	0.0700	3.5500	-0.2042
	C	0.0700	3.5500	-0.3350
	N	0.1700	3.2500	-0.3350
	H	0.0300	2.4200	+0.1629
$C_2H_4O_2$	C1	0.0660	3.5000	-0.3389
	C2	0.0700	3.5500	+0.4630
	O1	0.2100	2.9600	-0.3967
	O2	0.1700	3.1200	-0.5589
	H1	0.0300	2.5000	+0.1263
	H2	0.0000	0.0000	+0.4525
Quartz	Oc23	0.0540	3.0914	-0.5500
	Si	0.0930	3.6972	+1.1000
	Oc24	0.1220	3.0914	-0.6750
	Ho	0.0150	0.9667	+0.4000

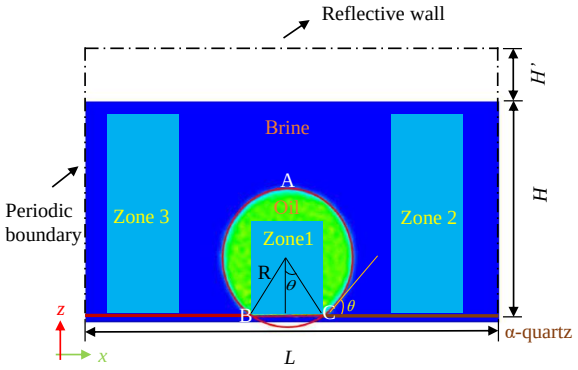

Fig. 2. Contact angle measurement in crude-oil-brine-quartz system with Zones 1-3 for local fluid properties.

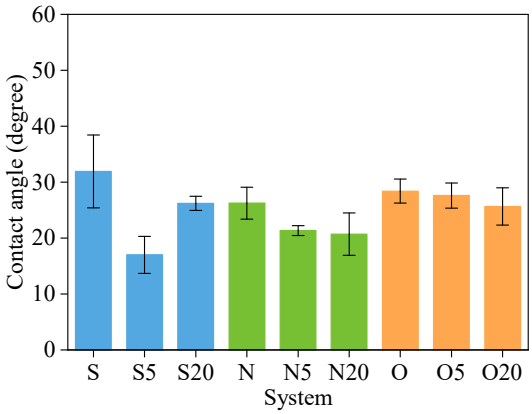

Fig. 3. Equilibrium contact angles of the crude oil-brine-quartz system under various conditions.

A custom MATLAB script was developed to identify three characteristic points (A, B and C) along the outer contour of the oil droplet for geometric fitting. In this procedure, the line connecting the intersection points between the outermost oil contour and the solution-substrate interface was defined as the three-phase contact line (BC line), ensuring the accurate calculation of the contact angle using Eq. (3). The length of the BC line is denoted as b. Finally, the average contact angle over the final 5 ns of the simulation was taken as the representative value for each system:

$$\theta = \arctan \frac{b/2}{\sqrt{R^2 - \frac{b^2}{4}}} \tag{3}$$

where θ denotes the contact angle, BC represents the distance between the two contact points of crude oil and the substrate, and R is the radius of the oil droplet. Hydrogen bonding was identified and quantified using the Hydrogen Bonds plugin in the VMD software package based on the geometric criteria established by Luzar and Chandler (1996).

3. Results and discussion

3.1 Change in contact angle

Using the contact angle calculation method described previously, the crude oil density distributions at varying dilution

levels were analyzed and the average contact angle for each system was determined, as shown in Fig. 3. The mean contact angles for the S-containing systems S, S5 and S20 were 31.9°, 17.1° and 26.2°, respectively. For the N-containing systems N, N5 and N20, the corresponding values were 26.3°, 21.3° and 20.7°, while the O-containing systems O, O5 and O20 exhibited contact angles of 28.4°, 27.6° and 25.7°, respectively.

With increasing dilution, all three oil types exhibited a general decrease in contact angle, with the most pronounced change observed in the S5 system. Furthermore, the variation in contact angle among the different crude oil types at identical brine concentrations suggests that wettability is influenced not only by brine salinity but also by the polarity of crude oil components. Specifically, acetic acid in the O-containing system, which contains highly polar carboxyl groups, exhibited stronger polarity than pyridine (N-containing) and mercaptan (S-containing) molecules. In principle, stronger polarity enhances interactions with the quartz surface, promoting adsorption and thus increasing the contact angle. However, this expected trend was not clearly manifested in the results, which may stem from the inherently strong hydrophilicity of the quartz substrate that could override the effects of molecular polarity. Furthermore, the simplified crude oil models employed may not fully capture the complexity of real crude oils, as they lack high-molecular-weight species such as resins and asphaltenes. To more comprehensively elucidate the role of polarity, future studies incorporating more chemically diverse oil components are warranted. Nonetheless, the observed contact angles, ranging from 15° to 35°, were consistent with the strong water-wet characteristics of quartz (Liu et al., 2024).

3.2 Fluid density distribution

To describe the interfacial distribution characteristics of fluid components and their impact on contact angles across various crude oil-brine systems, the fluid density along the z-axis was analyzed in three representative regions (Fig. 2). To represent the distribution near the quartz surface, the brine density in Regions 2 and 3 was averaged.

3.2.1 Water density

The density distribution of water molecules on the wall surface provides a direct reflection of changes in the hydrophilicity of the quartz substrate before and after brine dilution. Fig. 4 presents the average density profiles of water, consistent with prior findings by Zhan et al. (2020), where all systems exhibit distinct layering of water molecules near the quartz surface due to strong surface-fluid interactions. Two pronounced peaks appear at 2.8 Å and 5.8 Å from the surface, with corresponding densities of approximately 1.18 g/cm^3 and 1.00 g/cm^3, respectively. Beyond 8.8 Å, water molecules transition into the bulk phase, where the density stabilizes at $\sim$0.97 g/cm^3, indicating diminished quartz-water interactions. Notably, under undiluted brine conditions, all systems exhibit reduced water densities, particularly in the bulk region. This reduction can be attributed to the high ionic strength of the formation water, which disrupts hydrogen bonding between water molecules and increases intermolecular distances. Interestingly, while 20-fold dilution results in a higher bulk water density than 5-fold dilution, the near-surface water densities remain similar. This observation suggests that the adsorption of water molecules onto the quartz surface may reach saturation at the 5-fold dilution level.

The atomic trajectory analysis of fluid configurations across systems reveals the formation of a thin water film beneath the oil droplet, which plays a key role in mediating surface wettability (Drummond and Israelachvili, 2004). As shown in Fig. 5, the water density distributions exhibit sharp peaks at $\sim$ 1.8 Å from the quartz surface under all brine conditions. For S-containing crude oil systems, the water film exhibits maximum density (0.51 g/cm^3) and thickness (8.8 Å) under 5-fold dilution. In contrast, the undiluted system yields a lower peak density (0.33 g/cm^3) and a thinner water film (5.8 Å), while the 20-fold dilution condition results in intermediate values. These findings align with the minimum contact angle observed for the S5 system (Fig. 3), confirming that maximum water film development corresponds to enhanced water-wetness. For N-containing crude oil, the water film reaches its greatest density (0.58 g/cm^3) and thickness (9.8 Å) at the 20-fold dilution, compared to 0.41 g/cm^3 and 6.8 Å in the undiluted case. Similarly, in the O-containing crude oil system, water film density and thickness increase from 0.32 g/cm^3 and 5.8 Å (undiluted) to 0.53 g/cm^3 and 6.8 Å (20-fold dilution), again reflecting stronger water affinity at lower brine concentrations.

Collectively, these results reveal that both water film density and thickness increase as brine salinity decreases, due to the reduced disruptive effect of ions on water molecule mobility and hydrogen bonding. This facilitates the formation of a continuous water layer beneath the oil droplet, enhancing the hydrophilicity of the quartz surface. Correlation with contact angle data confirmed that thicker and denser water films lead to more water-wet surfaces.

3.2.2 Crude oil density

Wettability behavior is fundamentally influenced by the competitive adsorption of oil and water molecules on the substrate surface. To investigate the variation in crude oil adsorption strength before and after brine dilution, the one-dimensional density distributions of the three crude oil components along the z-axis under different brine dilution levels were determined, as shown in Fig. 6. Across all systems, three distinct adsorption peaks are observed in proximity to the quartz surface, with the first and second peaks located at 3.8 Å and $\sim$ 7.8 Å, respectively, and a markedly reduced third peak appearing at $\sim$ 12.8 Å. Beyond this value, the oil phase enters the bulk region where molecular distributions become insensitive to brine concentration. Notably, oil molecules accumulate predominantly at the first peak, directly above the interfacial water layer, as indicated by the density profiles.

For S-containing crude oil, the density of molecules adsorbed onto the quartz surface decreases significantly upon 5-fold dilution, coinciding with the maximum water film density. The formation of a robust water layer inhibits oil-surface interactions, displacing oil molecules further from the surface.

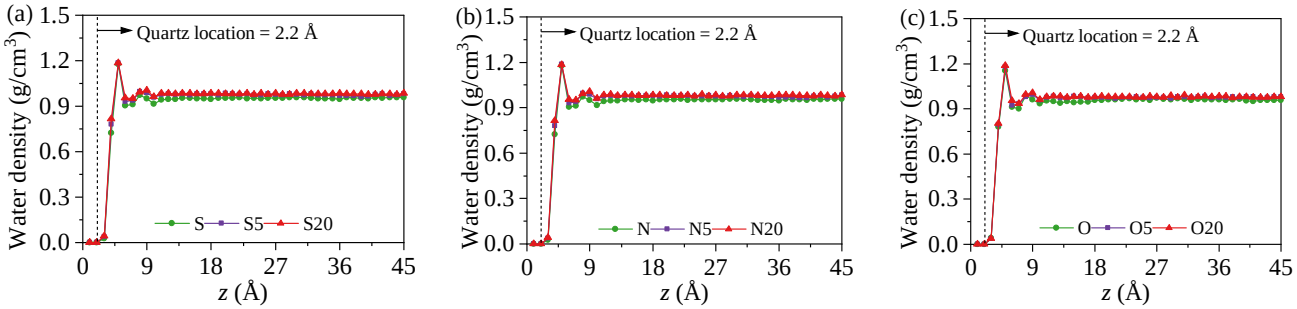

Fig. 4. One-dimensional average density distribution of water molecules along the *z*-axis in Regions 2 and 3 for crude oil systems containing (a) sulfur, (b) nitrogen and (c) oxygen under different brine dilutions.

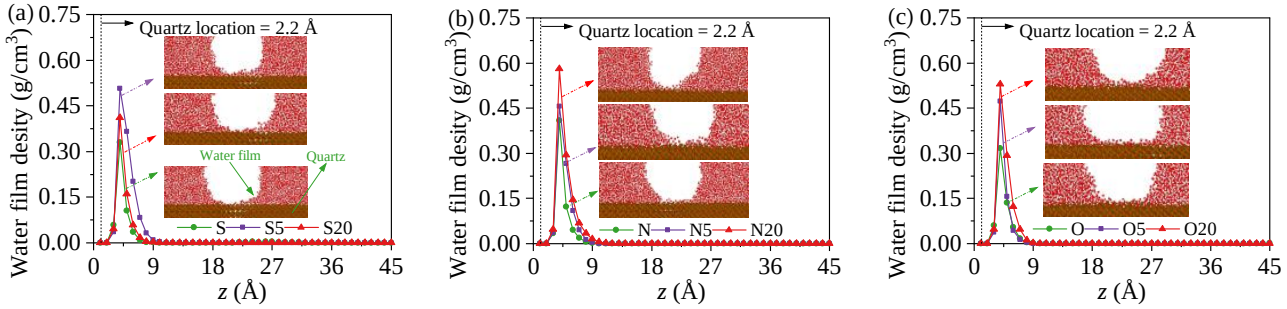

Fig. 5. One-dimensional density distribution of water film along the *z*-axis in Region 1 for crude oil systems containing (a) sulfur, (b) nitrogen and (c) oxygen under different brine dilutions.

In contrast, under undiluted conditions, limited water film formation allows for stronger oil-surface adhesion, resulting in a higher local oil density. A similar trend is observed in N-containing crude oil systems, where brine dilution enhances water adsorption onto the quartz surface, gradually displacing oil molecules. However, the extent of this displacement is not significant, reflected in only slight reductions in oil density. For O-containing crude oil, the highest oil density occurs under undiluted conditions, consistent with the largest contact angle. In the 20-fold diluted case, oil density is minimized, coinciding with the highest water film density and the smallest contact angle, reaffirming the inverse relationship between water film formation and oil-surface affinity.

To investigate the spatial distribution of oil components, the one-dimensional density profiles of alkanes were depicted in Fig. 7. In all crude oil systems, alkanes display two primary peaks near the quartz surface. The peak intensity difference is small in S- and N-containing systems, whereas O-containing systems exhibit a second peak that exceeds the first, indicating that alkanes are depleted near the wall. This suggests that interactions with the interfacial water film or other components inhibit alkane adsorption onto the mineral surface.

The density distributions of the aromatic components are further presented in Fig. 8. The aromatics consistently exhibit unimodal density profiles, indicating their preferential accumulation at the interface region. The insets with red circles reveal that some aromatic molecules are dispersed into the bulk oil phase as monomers or small aggregates, consistent with previous MD simulations (Sedghi et al., 2013). In S-containing crude oil, aromatic density peaks at 2.8 Å – beneath the alkane density maxima—implying competition for adsorption sites that contributes to alkane depletion near the surface. Meanwhile, in N-containing systems, the position of the aromatic peak shifts with brine dilution, suggesting unstable adsorption behavior. For O-containing systems, the aromatic peak migrates away from the quartz surface under dilution. Overlaying Fig. 7(c) further confirms the partial overlap between aromatic and alkane densities between 3.8 to 5.8 Å; however, no clear correlation between aromatic density and contact angle is evident, corroborating earlier findings (Khovental et al., 2025).

Non-hydrocarbon components represent the most polar constituents in the crude-oil model used in this study, whose one-dimensional density distributions under different brine dilution conditions are presented in Fig. 9. The three insets depict the spatial distributions of non-hydrocarbon molecules within the aqueous phase. To clearly visualize the spatial correspondence between non-hydrocarbon species and water molecules, the latter are shown with a blue background. Combining the insets with the one-dimensional density profiles, it is evident that these species are also predominantly concentrated in the interfacial region. Pyridine forms the thickest adsorption layer among the three, attributed to its higher interfacial activity and ability to form strong interactions with water. In contrast, mercaptan molecules in S-containing systems exhibit a lower peak density due to their

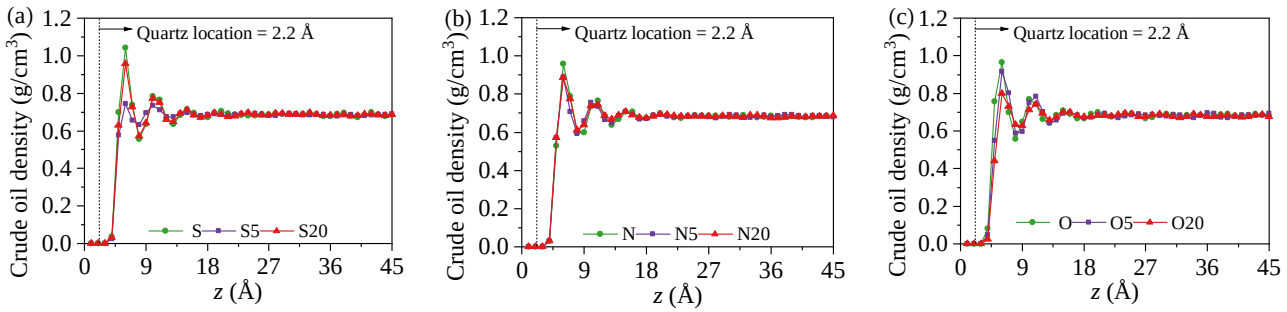

Fig. 6. One-dimensional density distribution of crude oil along the z-axis in Region 1 for crude oil systems containing (a) sulfur, (b) nitrogen and (c) oxygen under different brine dilutions.

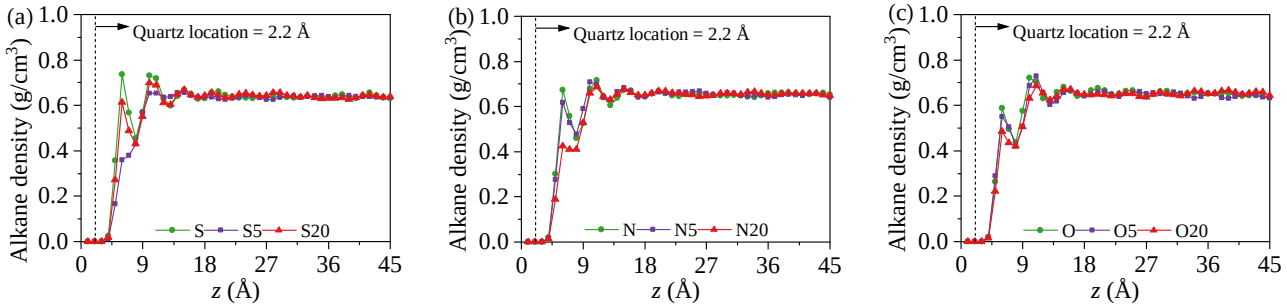

Fig. 7. One-dimensional density distribution of alkanes along the z-axis for Region 1 for crude oil systems containing (a) sulfur, (b) nitrogen, and (c) oxygen under different brine dilutions.

long hydrophobic alkyl chains and weak polarity, making them preferentially soluble in the hydrocarbon phase. The inset in Fig. 9(a) shows that some mercaptan molecules migrate into the bulk oil phase, highlighting their weak and unstable adsorption onto the hydrophilic quartz surface. In N-containing systems (Fig. 9(b)), brine dilution leads to increased pyridine adsorption, with density peaks shifting closer to the quartz surface. However, these remain above the water film layer, as verified by the water density profiles. Acetic acid molecules in O-containing crude oil (Fig. 9(c)) exhibit strong surface affinity due to their high polarity, consistently forming a stable adsorption peak at 2.8 Å. Unlike pyridine, the location of this peak remains unchanged across dilution conditions. However, the peak intensity declines with increasing dilution, nearly vanishing under 20-fold dilution. This trend is driven by competitive adsorption: as the interfacial water film thickens with brine dilution, water molecules increasingly occupy available adsorption sites, displacing acetic acid into the aqueous phase, as seen in the inset. This complete solubilization of acetic acid into the brine corresponds with maximal quartz hydrophilicity.

A comparative analysis of Figs. 9(b) and 9(c) reveals that acetic acid adsorption is more sensitive to brine dilution than pyridine. This is due to the stronger polarity and higher affinity of acetic acid for both quartz and water, resulting in a stronger competition with water molecules for adsorption sites. Lastly, a correlation is observed between non-hydrocarbon density and contact angle: in S- and O-containing systems, greater non-hydrocarbon adsorption corresponds to higher contact angles, while in N-containing systems, an inverse relationship is observed.

3.3 Radial distribution function

The radial distribution function, described by $g(r)$, quantifies the probability of locating a target particle at a specific distance from a reference particle, providing critical insights into the strength of intermolecular interactions and thus the underlying mechanisms governing wetting behavior changes upon brine dilution. In this study, $g(r)$ was computed between hydroxyl groups on the quartz surface and selected crude oil components (aromatics and non-hydrocarbons), as alkanes exhibited negligible wall interactions and lacked pronounced adsorption structures across all conditions. The corresponding results are presented in Fig. 10. Fig. 10(a) illustrates that aromatic molecules in S-containing crude oil exhibit stronger interactions with surface hydroxyl groups. A comparison with the density distributions of aromatic and non-hydrocarbon molecules in Figs. 8(a) and 9(a) indicates that this behavior can be attributed to their spatial proximity to the quartz surface. The $g(r)$ peak of aromatic molecules progressively diminishes with increasing dilution, indicating a weakening interfacial interaction. Fig. 10(b) depicts that in N-containing crude oil, the radial distribution function $g(r)$ peaks for both aromatic and non-hydrocarbon molecules increase with brine dilution, albeit with no distinct peaks formed, reflecting relatively weak adsorption. Notably, the trend of $g(r)$ changes for non-hydrocarbon molecules upon dilution is consistent with the

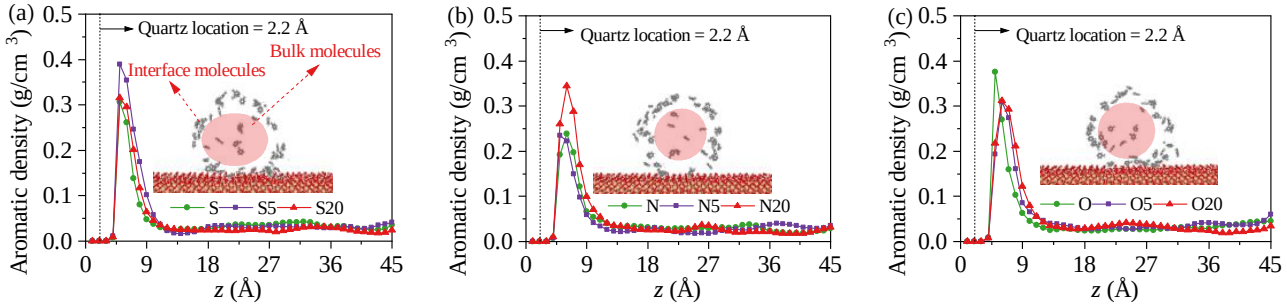

Fig. 8. One-dimensional density distribution of aromatics along the z-axis in Region 1 for crude oil systems containing (a) sulfur, (b) nitrogen and (c) oxygen under different brine dilutions.

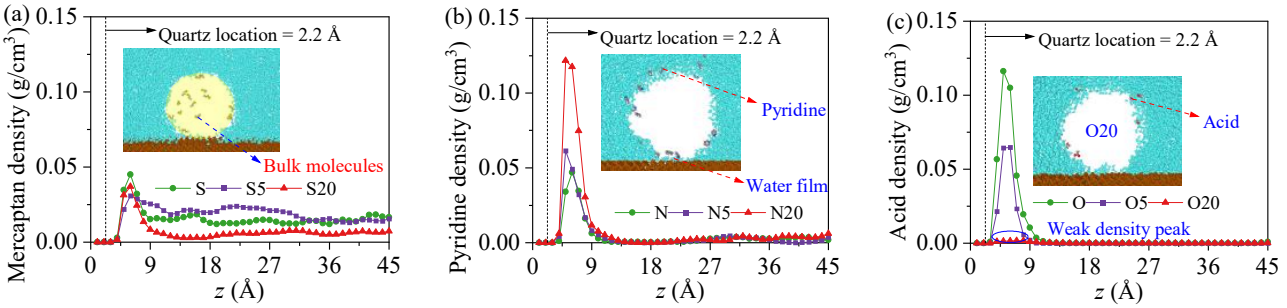

Fig. 9. One-dimensional density distribution of non-hydrocarbons along the z-axis in Region 1 for crude oil systems containing (a) sulfur, (b) nitrogen and (c) oxygen under different brine dilutions.

corresponding density distributions shown in Fig. 9(b) and exhibits a negative correlation with the observed contact-angle variations. In the O-containing crude oil system (Fig. 10(c)), non-hydrocarbon molecules exhibit strong adsorption onto quartz, with $g(r)$ peaks declining upon dilution, consistent with the reduction in non-hydrocarbon density on the surface. This observation also explains the gradual decrease in the density peak of acetic acid molecules with brine dilution, as shown in Fig. 9(c). Aromatics exhibit lower $g(r)$ values across all dilution levels. Notably, even at 20-fold dilution, acetic acid molecules retain a weak interaction with the quartz surface, corroborated by the density profiles in Fig. 9(c). These $g(r)$ trends align with the spatial density variations in aromatic and non-aromatic molecules discussed in Section 3.2. Overall, in various systems, the comparable magnitudes of $g(r)$ for aromatics and non-hydrocarbons suggest competitive adsorption on the quartz surface.

Furthermore, as depicted in Figs. 10(d)-10(f), the $g(r)$ peak between hydroxyl groups and water molecules reaches its maximum at the 5-fold dilution in the S-containing system, reflecting the strongest surface hydration under this condition and explaining the previously observed water density increases across the interfacial regions. In the N- and O-containing systems, the $g(r)$ peak between surface hydroxyl groups and water molecules increases with brine dilution, consistent with the trend of water density peaks near the substrate shown in Figs. 4(b)-4(c), indicating enhanced quartz hydrophilicity. This also explains the decrease in contact angle observed for N- and O-containing crude oils upon dilution (Fig. 3). In contrast, the corresponding $g(r)$ peak for acetic acid declines, reflecting competitive adsorption that favors water molecules as the brine becomes more dilute. Finally, Figs. 10(g)-10(i) reveal the hydration behavior of ions, following the order Ca^{2+} > Na^{+} > Cl^{-}, consistent with previous studies (Tian et al., 2015). Divalent Ca^{2+} forms two distinct hydration shells, with water molecules in the primary shell displaying greater order and stronger binding. In contrast, hydration shells around Na^{+} and Cl^{-} are looser, highlighting the superior hydration strength of Ca^{2+}. Upon 20-fold dilution, a slight increase in ion-water $g(r)$ peaks is observed, likely due to the increased interionic spacing that enables more stable hydration structures. Importantly, no evidence is found for strong ion adsorption onto the quartz surface. Overall, the $g(r)$ analysis indicates that the wettability of the crude oil-water-quartz interface is primarily governed by interactions between surface hydroxyl groups and water molecules. Across different conditions, the variations in hydroxyl-water $g(r)$ closely mirror the trends observed in the contact-angle measurements shown in Fig. 3.

3.4 Interaction energy

The interaction energy variation between system components can reflect the strength and nature of intermolecular interactions: negative values correspond to attractive interactions, with larger magnitudes indicating stronger adsorption, while positive values signify repulsive forces. As illustrated in Fig. 11, the brine-quartz interaction exhibits remarkable

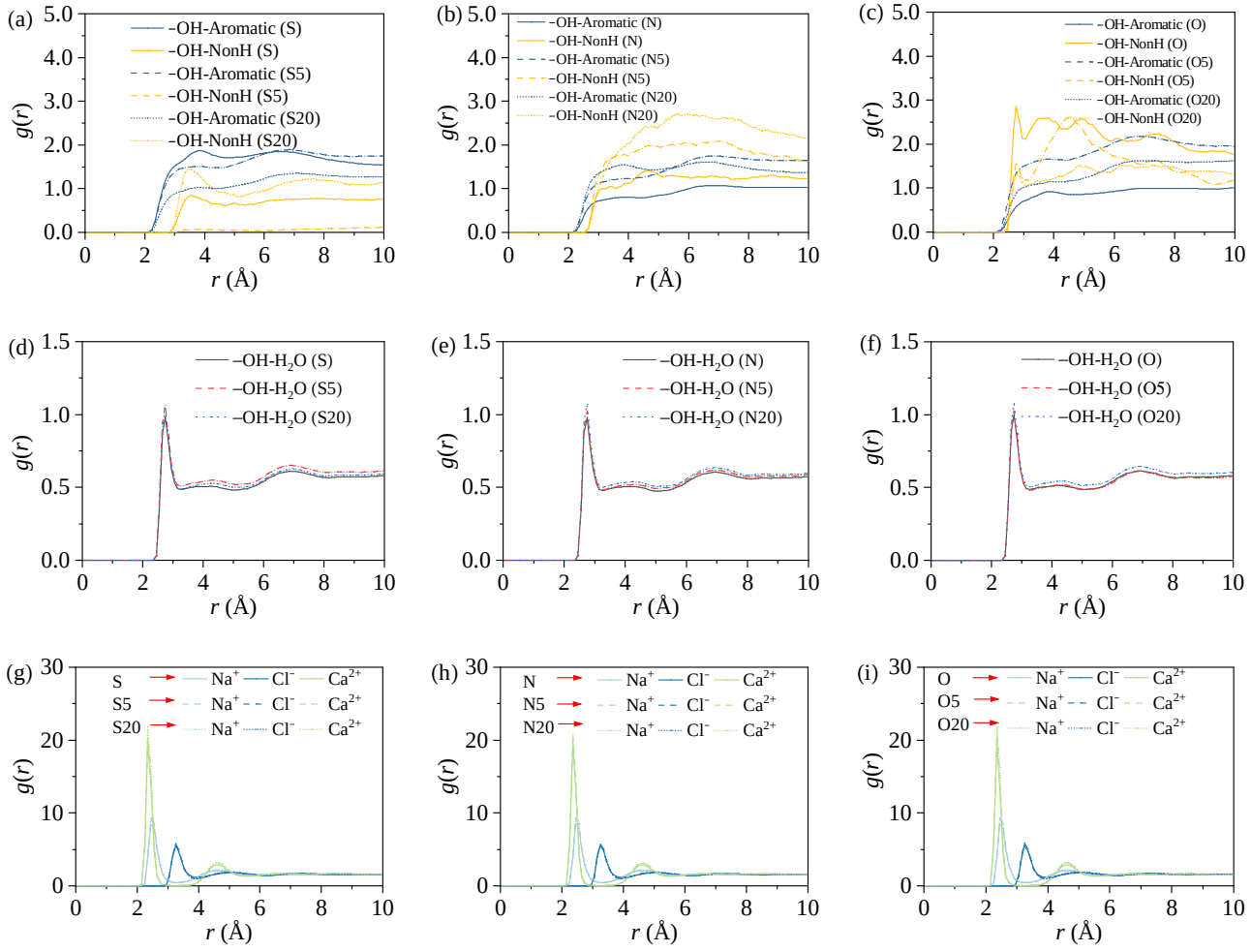

Fig. 10. Panels (a-c) present the radial distribution functions $g(r)$ between aromatic and non-hydrocarbon (NonH) components and hydroxyl groups on the quartz surface; Panels (d)-(f) illustrate the $g(r)$ between water molecules and quartz hydroxyl groups; Panels (g)-(i) depict the $g(r)$ between ions and water molecules under different crude oil systems and brine dilutions.

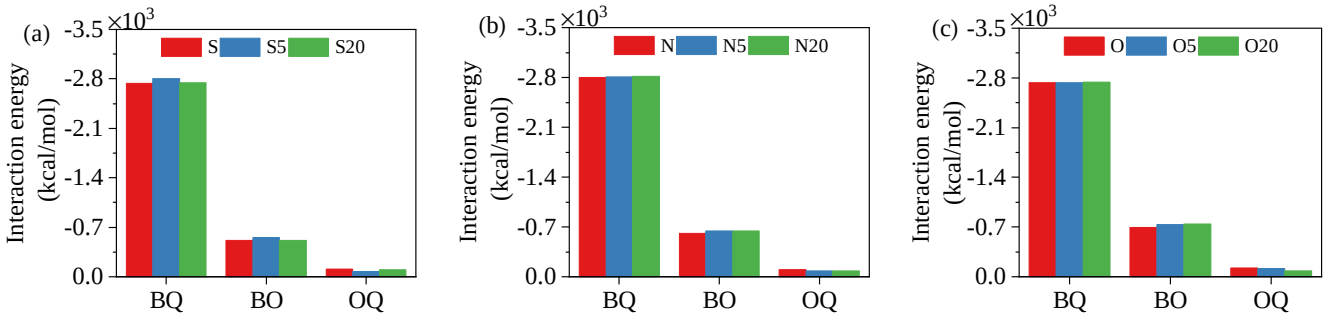

Fig. 11. Changes in interaction energy between brine and quartz (BQ), brine and oil (BO), and oil and quartz (OQ) in (a) the S-containing crude oil systems, (b) the N-containing crude oil systems, and (c) the O-containing crude oil systems.

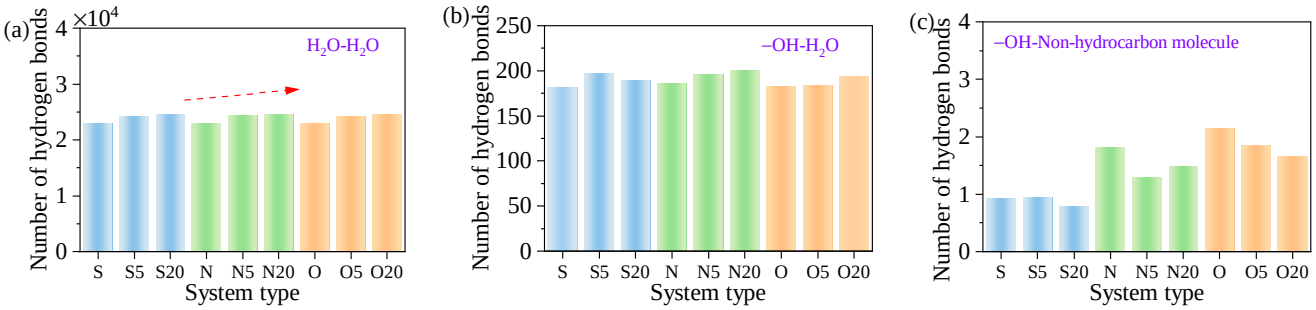

Fig. 12. Number of hydrogen bonds formed (a) between water molecules, (b) between water molecules and hydroxyl groups on the quartz surface, and (c) between heteroatoms and quartz surface hydroxyl groups across different systems.

adsorption energy across all systems, primarily due to the strong hydrophilicity of the quartz surface and the extensive contact area between brine and quartz under the simulated conditions. Specifically, Fig. 11(a) shows that the largest adsorption energy for brine-quartz corresponds to the 5-fold dilution condition. This enhanced interaction leads to the formation of the densest water film at the solid-liquid interface, which in turn weakens the adsorption of crude oil molecules onto the quartz surface by occupying favorable adsorption sites. As a result, the interaction energy between crude oil and quartz becomes less negative, consistent with the observed reduction in crude oil density near the wall surface. In contrast, Figs. 11(b)-11(c) reveal that while the brine-quartz interaction energy shows a slight increase with further dilution in the N- and O-containing crude oil systems, the overall variation is minimal. This also results in only minor modulation of the crude oil-quartz interaction energy, indicating that in these systems, the effect of brine on oil adsorption is not pronounced.

A broader analysis reveals an inverse relationship of the adsorption energy between the brine and crude oil and that between the crude oil and quartz. This inverse trend can be attributed to the competitive nature of interfacial interactions, wherein enhanced brine adsorption diminishes the availability of quartz surface sites for crude oil attachment. Notably, this behavior aligns with the relatively small variations in contact angle observed across different dilution conditions, suggesting that the adsorption energy between brine and crude oil is primarily modulated by structural changes in the underlying water film.

3.5 Analysis of hydrogen bonds

Hydrogen bonding plays a critical role in modulating interfacial interactions, particularly through bonds formed between water molecules and more electronegative atoms. To elucidate these effects, the number of hydrogen bonds was calculated under various conditions: that between water molecules, that between water molecules and surface hydroxyl groups of quartz, and that between quartz hydroxyl groups and non-hydrocarbon components of crude oil (see Fig. 12). As shown in Fig. 12(a), the number of hydrogen bonds between water molecules increases significantly with brine dilution. This trend arises from the reduced ionic strength, which lessens the disruption of the hydrogen-bond network by dissolved ions and thereby promotes the formation of a more extensive and coherent H-bonded water structure. Fig. 12(b) reveals that in N- and O-containing crude oil systems, brine dilution enhances the formation of hydrogen bonds between quartz surface hydroxyl groups and water molecules. This indicates stronger interfacial interactions between water and the quartz surface, leading to increased water adsorption, greater surface hydrophilicity, and a corresponding reduction in the contact angle. In the S-containing crude oil system, the number of hydrogen bonds with water also increases upon 20-fold dilution. However, the most pronounced increase occurs at 5-fold dilution, coinciding with the lowest observed contact angle. This suggests that a moderate dilution level optimally enhances interfacial hydration and displaces crude oil from the surface more effectively. In contrast, the increase in H-bond formation upon dilution is relatively modest in the N- and O-containing systems, consistent with the smaller reductions in contact angle observed for these systems. As depicted in Fig. 12(c), the number of hydrogen bonds between quartz hydroxyl groups and non-hydrocarbon molecules is significantly lower, which is due to the limited proportion of such components in the crude oil. Among the non-hydrocarbon species, acetic acid forms more hydrogen bonds with the quartz surface than pyridine, attributed to its higher polarity and stronger hydrogen-bonding capacity. Notably, in the S-containing crude oil system, the low number of hydrogen bonds is partly due to the migration of hydrophobic mercaptan molecules into the bulk oil phase, thereby reducing their interaction with the quartz surface.

The above analysis primarily focuses on the changes in the average number of hydrogen bonds after different systems reach equilibrium. Given that hydroxyl-water hydrogen bonding is the dominant factor governing differences in contact angle, the present study further analyzed the dynamic evolution of hydrogen bonds between hydroxyl groups and water molecules throughout the entire simulation. The results indicated that hydrogen bonds form within a very short time and their number exhibits only minor fluctuations over the course of the simulation, showing limited dependence on brine composition or simulation time. In addition, hydrogen-bond lifetime analyses were performed, revealing that brine dilution

alters interfacial molecular coverage, aggregation and disaggregation dynamics, and solute-water interactions, thereby affecting both the number of hydrogen bonds and their formation dynamics. Notably, hydrogen-bond lifetime does not correlate directly with the instantaneous number of hydrogen bonds. Detailed analyses are provided in the Supporting Materials.

3.6 Further implications

The findings of this study provide important insights for the practical implementation of low-salinity water injection techniques in enhanced oil recovery. First, our results suggest that in water-wet reservoirs, brine dilution may exert limited influence on wettability alteration, which helps to explain the inconsistent performance of low-salinity water injection observed in laboratory experiments (Bartels et al., 2019). Notably, the response of contact angle to dilution is not universally monotonic: while N- and O-containing crude oils exhibit a consistent decrease in contact angle with dilution, S-containing systems display a non-monotonic trend. This observation offers a mechanistic explanation for the existence of an optimal salinity in various experimental and field conditions. Second, under certain conditions, such as the 20-fold dilution scenario (O20), non-hydrocarbon species are almost completely absent from the oil-quartz interface, highlighting the capacity of brine dilution to modulate the interfacial distribution of O-containing molecules, particularly small polar compounds. This suggests that in oils dominated by O-containing non-hydrocarbons, tuning interfacial tension via salinity control may be an especially effective strategy. Third, the complexity of crude oil composition introduces additional challenges. For systems rich in heavy polar fractions, such as resins and asphaltenes, further investigation is required to assess how brine dilution influences interfacial structure and wettability. This is especially relevant for unconventional reservoirs, where interactions with clay minerals and nanoscale pore surfaces could significantly alter interfacial behavior. A comprehensive understanding of these interactions will be essential to optimize low-salinity water injection in such reservoirs.

4. Conclusions

Using MD simulations, this study elucidates the microscopic mechanisms by which brine dilution alters interfacial behavior in crude oil-brine-quartz systems, focusing on the roles of S-, N- and O-containing polar components. The key findings are summarized as follows:

1) Brine dilution generally enhances system hydrophilicity. For N- and O-containing crude oils, the contact angle decreases monotonically with increasing dilution, whereas S-containing systems exhibit a non-monotonic variation. Nonetheless, the overall changes in contact angle are minor across all cases.
2) A water film separates the oil phase from the quartz surface. As brine is diluted, the film becomes thicker, which lowers the crude oil density near the surface, weakens the oil-quartz interactions, and thereby reduces the contact angle.
3) The spatial distribution of crude oil components near the interface varies by molecular type: alkanes are depleted from the quartz surface, aromatics preferentially localize at the interface, and in S-containing oils, they are positioned closer to the surface than non-hydrocarbons. Importantly, the correlation between non-hydrocarbon surface density and contact angle differs by oil type: it is positive in O- and S-containing systems but negative in N-containing systems.
4) Brine dilution increases water adsorption on the quartz surface, as evidenced by higher $g(r)$ peaks, stronger interaction energies, and increased hydrogen bond formation. This effect is most pronounced in the 5-fold dilution of S-containing oil, which also exhibits the largest contact angle reduction. In contrast, other dilution levels result in weaker responses.

In summary, brine dilution promotes water-quartz interactions and suppresses oil-quartz adhesion, collectively enhancing surface water wettability and slightly reducing the contact angle. However, because the initial system is already strongly hydrophilic, the extent of contact angle change remains limited. This constraint may reduce the effectiveness of low-salinity water injection in improving oil recovery in water-wet reservoirs, underscoring the need for targeted application strategies based on oil composition and initial wetting conditions.

Acknowledgements

The authors would like to acknowledge the support of the National Natural Science Foundation of China (No. 52204044), the Youth Innovation Team of Shaanxi Universities (No. 23JP131), and the Postgraduate Innovation Fund Project of Xi'an Shiyou University (No. YCX2412013).

Supplementary file

https://doi.org/10.46690/capi.2026.01.02

Conflicts of interest

The authors declare no competing interest.

References

Aljamali, N. M., Salih, N. S. Review on chemical separation of crude oil and analysis of its components. Journal of Petroleum Engineering & Technology, 2021, 11(2): 35-49.

Almeida da Costa, A., Trivedi, J., Soares, J., et al. An experimental evaluation of low salinity water mechanisms in a typical brazilian sandstone and light crude oil with low acid/basic number. Fuel, 2020, 273: 117694.

Alomair, O., Al-Dousari, M., Azubuike, N., et al. Evaluation of the impact of low-salinity water on wettability alteration and oil recovery in berea sandstones. Fuel, 2023,

337: 127151.

Arain, A. H., Negash, B. M., Farooqi, A. S., et al. Improving oil recovery through low salinity waterflooding and nanoparticles: A mini review. Energy & Fuels, 2024, 38(18): 17109-17127.

Arboleda-Lamus, A., Muñoz-Rugeles, L., del Campo, J. M., et al. Salinity and ph effects on water-oil-calcite interfaces by using molecular dynamics. Physical Chemistry Chemical Physics, 2024, 26(19): 14393-14406.

Bartels, W.-B., Mahani, H., Berg, S., et al. Literature review of low salinity waterflooding from a length and time scale perspective. Fuel, 2019, 236: 338-353.

Bhutto, D. K., Shar, A. M., Abbasi, G. R., et al. Shale wettability characteristics via air/brines and air/oil contact angles and influence of controlling factors: A case study of lower indus basin, Pakistan. ACS Omega, 2022, 8(1): 688-701.

Cai, J., Jiao, X., Wang, H., et al. Multiphase fluid-rock interactions and flow behaviors in shale nanopores: A comprehensive review. Earth-Science Reviews, 2024, 257: 104884.

Cai, J., Jin, T., Kou, J., et al. Lucas-washburn equation-based modeling of capillary-driven flow in porous systems. Langmuir, 2021, 37(5): 1623-1636.

Chen, S. H., Singer, S. J. Molecular dynamics study of the electric double layer and nonlinear spectroscopy at the amorphous silica water interface. Journal of Physical Chemistry B, 2019, 123(29): 6364-6384.

Chen, Z., Lin, J., Wang, W., et al. Insights into wettability alteration mechanisms of microbial enhanced oil recovery by different biosurfactants in sandstone oil reservoir. Colloids and Surfaces A: Physicochemical and Engineering Aspects, 2024, 691: 133889.

Cheng, Z., Tong, S., Wang, D., et al. Experimental investigation on the interfacial characteristics of tight oil rocks induced by tuning brine chemistry. ACS Omega, 2024, 9(28): 30654-30664.

Cheng, Z., Tong, S., Zhang, S., et al. Effects of high concentration of Mn^{2+} on wettability of tight sandstones: Experimental and molecular insights. SPE Journal, 2025, 30(12): 7690-7702.

Cui, F., Jin, X., Liu, H., et al. Molecular modeling on gulong shale oil and wettability of reservoir matrix. Capillarity, 2022, 5(4): 65-74.

Dastjerdi, A. M., Kharrat, R., Niasar, V., et al. Salinity-driven structural and viscosity modulation of confined polar oil phases by carbonated brine films: Novel insights from molecular dynamics. The Journal of Physical Chemistry B, 2024, 128(7): 1780-1795.

Deng, Y., Li, Z., Rao, S., et al. Mechanism for the effects of surface chemical composition and crystal face on the wettability of α-quartz surface. Applied Surface Science, 2023, 633: 157559.

Dordzie, G., Dejam, M. Enhanced oil recovery from fractured carbonate reservoirs using nanoparticles with low salinity water and surfactant: A review on experimental and simulation studies. Advances in Colloid and Interface Science, 2021, 293: 102449.

Drummond, C., Israelachvili, J. Fundamental studies of crude oil-surface water interactions and its relationship to reservoir wettability. Journal of Petroleum Science and Engineering, 2004, 45(1-2): 61-81.

Fang, B., Zhang, Z., Zhang, Q., et al. Molecular insights into two-phase flow in clay nanopores during gas hydrate recovery: Wettability-induced multiple pathways of water lock formation. Advances in Geo-energy Research, 2025, 17(1): 17-29.

Fang, C., Yang, Y., Sun, S., et al. Low salinity effect on the recovery of oil trapped by nanopores: A molecular dynamics study. Fuel, 2020, 261: 116443.

Ghasemi, M., Shafiei, A. Atomistic insights into role of low salinity water on montmorillonite-brine interface: Implications for eor from clay-bearing sandstone reservoirs. Journal of Molecular Liquids, 2022, 353: 118803.

Ghasemi, M., Shafiei, A., Foroozesh, J. A systematic and critical review of application of molecular dynamics simulation in low salinity water injection. Advances in Colloid and Interface Science, 2022, 300: 102594.

Gómez-Delgado, J. L., Rodriguez-Molina, J. J., Perez-Angulo, J. C., et al. Evaluation of the wettability alteration on sandstone rock by graphene oxide adsorption. Emergent Materials, 2023, 7(5): 2045-2054.

Heinz, H., Lin, T.-J., Kishore Mishra, R., et al. Thermodynamically consistent force fields for the assembly of inorganic, organic, and biological nanostructures: The interface force field. Langmuir, 2013, 29(6): 1754-1765.

Javadi, A. H., Fatemi, M. Impact of salinity on fluid/fluid and rock/fluid interactions in enhanced oil recovery by hybrid low salinity water and surfactant flooding from fractured porous media. Fuel, 2022, 329: 125426.

Khalkhali, M., Kazemi, N., Zhang, H., et al. Wetting at the nanoscale: A molecular dynamics study. The Journal of Chemical Physics, 2017, 146(11): 114704.

Khovental, P., Kopanichuk, I., Vishnyakov, A. Molecular simulation of quartz wetting in crude oil/brine system at reservoir conditions using a novel protocol for contact angle calculation. Colloids and Surfaces A: Physicochemical and Engineering Aspects, 2025, 708: 135978.

Kobayashi, K., Firoozabadi, A. Water film structure and wettability of different quartz surfaces: Hydrogen bonding across various cutting planes. Langmuir, 2024, 40(9): 4635-4645.

Koleini, M. M., Badizad, M. H., Kargozarfard, Z., et al. The impact of salinity on ionic characteristics of thin brine film wetting carbonate minerals: An atomistic insight. Colloids and Surfaces A: Physicochemical and Engineering Aspects, 2019, 571: 27-35.

Kunieda, M., Nakaoka, K., Liang, Y. F., et al. Self-accumulation of aromatics at the oil-water interface through weak hydrogen bonding. Journal of the American Chemical Society, 2010, 132(51): 18281-18286.

Liu, B., Lei, X., Ahmadi, M., et al. Surface modeling of wettability transition on α-quartz: Insights from experiments and molecular dynamics simulations. Journal of Molecular Liquids, 2024, 406: 125147.

Liu, S. Review of the development status and technology of

tight oil: Advances and outlook. Energy & Fuels, 2023, 37(19): 14645-14665.

Liu, S., Hubao, A., Tang, S., et al. Molecular insights into structural and dynamic properties of water molecules in calcium silicate hydrate nanopores: The roles of pore size and temperature. Capillarity, 2023, 8(2): 23-33.

Luzar, A., Chandler, D. Effect of environment on hydrogen bond dynamics in liquid water. Physical Review Letters, 1996, 76(6): 928-931.

Lyu, F., Ning, Z., Kang, Y., et al. Molecular dynamics simulations of shale wettability alteration and implications for CO_2 sequestration: A comparative study. Colloids and Surfaces A: Physicochemical and Engineering Aspects, 2024, 699: 134710.

Mohammed, S., Alsmaeil, A. W., Asgar, H., et al. Directing the adsorption and assembly of laponite nano-discs at oil-water interfaces. Nanoscale Advances, 2025, 7(11): 3396-3405.

Oguntade, T. I., Fadairo, A. S., Pu, H., et al. Experimental investigation of zwitterionic surfactant for enhanced oil recovery in unconventional reservoir: A study in the middle bakken formation. Colloids and Surfaces A: Physicochemical and Engineering Aspects, 2024, 700: 134768.

Pan, J., Jiao, F., Wang, K., et al. Molecular simulations of the effects of CO_2 and N_2 injection on CH_4 adsorption, coal porosity and permeability. Advances in Geo-energy Research, 2024, 12(3): 205-222.

Plimpton, S. Fast parallel algorithms for short-range molecular dynamics. Journal of Computational Physics, 1995, 117(1): 1-19.

Sedghi, M., Goual, L., Welch, W., et al. Effect of asphaltene structure on association and aggregation using molecular dynamics. The Journal of Physical Chemistry B, 2013, 117(18): 5765-5776.

Seyyedattar, M., Zendehboudi, S., Butt, S. Molecular dynamics simulations in reservoir analysis of offshore petroleum reserves: A systematic review of theory and applications. Earth-Science Reviews, 2019, 192: 194-213.

Shi, K. Y., Chen, J. Q., Pang, X. Q., et al. Wettability of different clay mineral surfaces in shale: Implications from molecular dynamics simulations. Petroleum Science, 2023, 20(2): 689-704.

Singh, D., Friis, H. A., Jettestuen, E., et al. Ripening of capillary-trapped CO_2 ganglia surrounded by oil and water at the pore scale: Impact of reservoir pressure and wettability. Energy & Fuels, 2024, 38(10): 8853-8874.

Stukowski, A. Visualization and analysis of atomistic simulation data with OVITO-the open visualization tool. Modelling and Simulation in Materials Science and Engineering, 2009, 18(1): 015012.

Sun, C., Zhu, S., Xu, S., et al. Molecular physics in ion-bridging effect for wettability alteration of rock surfaces. Chemical Physics Letters, 2021, 763: 138201.

Tang, X., Xiao, S., Lei, Q., et al. Molecular dynamics simulation of surfactant flooding driven oil-detachment in nano-silica channels. The Journal of Physical Chemistry B, 2018, 123(1): 277-288.

Tian, H., Chen, T., Ma, Q., et al. Wettability modification by surfactants and temperature in shale oil reservoir conditions. Journal of Molecular Liquids, 2024, 401: 124607.

Tian, H., Liu, F., Jin, X., et al. Competitive effects of interfacial interactions on ion-tuned wettability by atomic simulations. Journal of Colloid and Interface Science, 2019, 540: 495-500.

Tian, H., Wang, M. Molecular dynamics for ion-tuned wettability in oil/brine/rock systems. AIP Advances, 2017, 7(12): 125017.

Tian, R. U. I., Yang, G., Liu, X., et al. Observation of the unusual aggregation kinetics of colloidal minerals in acidic solutions. Journal of Chemical Sciences, 2015, 127(6): 1083-1089.

Wang, F., Chang, S. Molecular dynamics investigation of shale oil occurrence and adsorption in nanopores: Unveiling wettability and influencing factors. Chemical Engineering Journal, 2024, 481: 148380.

Wang, X., Wu, X., Shi, L., et al. Application of low-salinity waterflooding in heavy oil sandstone reservoir: Oil recovery efficiency and mechanistic study. ACS Omega, 2024, 9(28): 30782-30793.

Wang, L., Zhang, Y. F., Zou, R., et al. Applications of molecular dynamics simulation in studying shale oil reservoirs at the nanoscale: Advances, challenges and perspectives. Petroleum Science, 2025, 22(1): 234-254.

Zhan, S., Su, Y., Jin, Z., et al. Effect of water film on oil flow in quartz nanopores from molecular perspectives. Fuel, 2020, 262: 116560.